Journal of Solid State Chemistry 183 (2010) 2797–2804

Contents lists available at ScienceDirect

Journal of Solid State Chemistry

journal homepage: www.elsevier.com/locate/jssc

Microwave absorption properties and infrared emissivities of ordered mesoporous C–TiO_2 nanocomposites with crystalline framework

Tao Wang, Jianping He *, Jianhua Zhou, Jing Tang, Yunxia Guo, Xiaochun Ding, Shichao Wu, Jianqing Zhao

College of Material Science and Technology, Nanjing University of Aeronautics and Astronautics, Nanjing 210016, PR China

ARTICLE INFO

Article history:
Received 18 June 2010
Received in revised form
6 September 2010
Accepted 20 September 2010
Available online 24 September 2010

Keywords:
Mesoporous nanocomposite
Solvent-evaporation induced self-assembly
Microwave absorption
Infrared emissivity

ABSTRACT

Ordered mesoporous C–TiO_2 nanocomposites with crystalline framework were prepared by the evaporation-induced triconstituent co-assembly method. The products were characterized by XRD, TEM, N_2 adsorption–desorption and TG. Their microwave absorption properties were investigated by mixing the product and epoxy resin. It is found that the peak with minimum reflection loss value moves to lower frequencies and the ordered mesoporous C–TiO_2 nanocomposite possesses an excellent microwave absorbing property with the maximum reflection loss of −25.4 dB and the bandwidth lower than −10 dB is 6.6 GHz. The attenuation of microwave can be attributed to dielectric loss and their absorption mechanism is discussed in detail. The mesoporous C–TiO_2 nanocomposites also exhibit a lower infrared emissivity in the wavelength from 8 to 14 μm than that of TiO_2-free powder.

1. Introduction

Since the first discovery of ordered mesoporous silicates in 1992, a window to new technological areas has been opened [1,2]. Ordered mesoporous materials have received steady growing interest because of their fascinating properties and various applications as compared with the bulk or microsized counterparts [3–6]. Recently, the synthesis of carbon-based composite with uniform mesopores and high surface area received significant attention because they may have the advantages of coupling the function of non-carbon phase with the rich properties of carbon and the new and unpredictable properties [7,8]. Zhao et al. [9–11] synthesized the ordered carbon/oxides nanocomposites using the evaporation-induced triconstituent co-assembly method. The degradation of rhodamine B and the electrocatalytic properties of the ordered C–TiO_2 nanocomposites were demonstrated in their reports. He et al. [12,13] synthesized OMC-Ni as a catalyst support which can easily yield a higher mass activity when the initial Ni content is around 10–15% and OMC-NiO with an excellent capacitance properties because of the presence of NiO nanocrystallites.

Microwaves have been widely used in both military and civil applications: radar, space technology, telecommunication, local area networks, personal digital assistant, etc. [14,15]. However, there are many problems caused by the increasing usage of microwave. In order to provide solution to electromagnetic interference (EMI) and electromagnetic compatibility (EMC), the absorbers of microwave are becoming very important, which have attracted much attention of many scientists [16–19]. Generally, magnetic metal particles are used for the microwave absorption materials. However, the high specific gravity and the difficult formulation have limited their practical applications. The nanoscale materials have attracted increasing interest in microwave absorbing and shielding materials in the high-frequency range due to their many unique chemical and physical properties [20,21]. Particularly, the unique structures and many excellent properties of carbon nanotubes (CNTs) have prompted intensive studies for electromagnetic wave absorbing [22–24]. Many efforts have been focused on the combination of organic polymers or carbon with inorganic nanocrystals or metal nanoparticles in order to yield new functional material which may combine the advantages of each component [25–27]. Mesoporous titania-based materials with a crystalline framework, high surface area and tunable pore size have received significant research attention due to the range of applications for such materials: photocatalysis [28–30], sensing fields [31,32], energy storage and conversion [33,34]. Recently, PAni/HCl/TiO_2 nanocomposite fabricated by using TiO_2 as a filler showed a large dielectric constant [35]. Phang et al. reported a novel hexanoic acid (HA) doped PAni micro/nanocomposite containing TiO_2 and Fe_3O_4 and PAni/HA/TiO_2/Fe_3O_4 with 40% of Fe_3O_4 achieved the best performance of microwave absorption (greater than 99.4% absorption) at high frequency [36]. TiO_2 shows excellent transparency and stability, so TiO_2 is also expected to improve the infrared absorbing

* Corresponding author. Fax: +86 025 52112626.
E-mail address: jianph@nuaa.edu.cn (J. He).

0022-4596/$ - see front matter © 2010 Elsevier Inc. All rights reserved.
doi:10.1016/j.jssc.2010.09.028

performance, while not affecting the microwave absorbing performance of the material [37]. Ordered mesoporous carbon with TiO_2 as a dielectric filler could be an excellent microwave absorbing material, but few studies on their infrared emissivities and microwave absorbing behaviors have been carried out.

In this paper, ordered mesoporous C–TiO_2 nanocomposites with crystalline framework were synthesized by using a low-molecular-weight resol (phenol–formaldehyde, $M_w < 500$) as an organic precursor, less reactive metal alkoxide as an inorganic precursor, and amphiphilic triblock copolymer F127 as a template. Add amorphous components, such as carbon, into the mesostructured metal oxides framework, can form a glasslike phase; it is responsible for the stability of ordered mesostructures [10]. Moreover, the combination of ordered mesoporous structure and incorporation of TiO_2 may contribute to the better impedance matching, which can result in the improved microwave absorption in a wide band. We investigated the effect of annealing temperature on the crystalline state of TiO_2 and TiO_2/C ratio on the microwave adsorption performance of C–TiO_2 nanocomposites. Additionally, the infrared emissivities of C–TiO_2 nanocomposites were also investigated. The ordered mesoporous C–TiO_2 nanocomposites exhibit effective microwave adsorption performances and lower infrared emissivities in the wavelength from 8 to 14 μm.

2. Materials and methods

2.1. Materials

All the reagents were of analytical purity and used without further purification. Pluronic F127 (EO106PO70EO106, EO= ethylene oxide, PO=propylene oxide) was purchased from Sigma-Aldrich Corporation. Tetrabutyl titanate, phenol, formaldehyde, hydrofluoric acid, hydrochloric acid and ethanol were purchased from Sinopharm Chemical Reagent Limited Corporation. The resol precursor ($M_w < 500$) was prepared according to the procedure reported previously [38].

2.2. Synthesis

In a typical preparation, 2 g of Pluronic F127 was dissolved in 12 ml of absolute ethyl alcohol and stirred for 1 h at 40 °C as solution A. Meantime solution B was prepared from 1.5 ml of 37 wt% hydrochloric acid and 6 ml of absolute ethyl alcohol. Tetrabutyl titanate (3.4 g) was portioned slowly to solution B under vigorous stirring. After 1 h stirring, solution B and 2.5 g of 20 wt% resols' ethanolic solution were added in solution A. After being stirred for 2 h, the mixture was transferred into dishes. It took 24 h at room temperature to evaporate ethanol and 36 h at 70 °C in an oven to thermopolymerize. The as-made products, orange and transparent films, were scraped from the dishes. Calcination was carried out in a tubular furnace at 350 °C for 5 h and 500, 600 and 700 °C for 2 h under N_2 flow with a rate of 1 °C/min to remove the amphiphilic triblock copolymer templates and get mesoporous C–TiO_2 nanocomposites. We take the mesoporous nanocomposite C–TiO_2-x with x representing the heating temperature. Mesoporous nanocomposite C–TiO_2-350 was calcined at 350 °C for 5 h in air to burn off carbon and generate mesoporous titania material. The nanocomposites with different compositions in a wide range from 30 to 70 wt% TiO_2 were prepared by varying the mass ratios of resol to tetrabutyl titanate. The final products were labeled as MCyT$(10-y)$, where y represents the weight percentage of carbon content in the nanocomposites. Moreover, ordered mesoporous carbon (OMC-500) as a reference was prepared according to the previous report [39].

2.3. Characterization

The porous structures of the ordered mesoporous C–TiO_2 nanocomposites and mesoporous TiO_2 oxide were measured by N_2 adsorption–desorption isotherm using Micromeritics ASAP 2010 at 77 K. X-ray diffraction (XRD) patterns were recorded by a Bruker D8 ADVANCE diffractometer using Cu $K\alpha$ radiation (λ=0.154056 nm). Transmission electron microscopy (TEM, FEI Tecnai G^2) operating at 200 kV was applied to characterize the morphology of the mesoporous materials. Samples for TEM measurements were prepared by ultrasonically suspending the powder in ethanol and placing a drop of the suspension on a carbon film supported by Cu grids. Weight changes of the products were monitored using a Mettler Toledo TG-209-F1 analyzer (NETZSCH) from 25 to 950 °C under nitrogen or air with a heating rate of 5 °C min^{-1}. Energy dispersive X-ray spectrum (EDS) installed in FEI Tecnai G^2 system was also used to analyze the microzone composition of the samples.

2.4. Microwave adsorption measurement

The as-prepared powders were uniformly dispersed into the commercial epoxy resin and then pressed into toroidal-shaped samples with the outer diameter of 7.0 mm, the inner diameter of 3.04 mm and the thickness of 3.0 mm. Commercial epoxy resin [40,41] or paraffin [42,43] is often used as binder matrix in electromagnetic wave adsorption measurement. In order to study electromagnetic wave absorption properties systematically in our researches [44,45], we are familiar with commercial epoxy resin as binder matrix. The scattering parameters S_{11}, S_{21} of the samples with 40 wt% as-prepared powders were measured using a vector network analyzer (Agilent E8363A) by the coaxial reflection/transmission technique. The relative permittivity and permeability values were determined from the scattering parameters as measured in the frequency range 0.5–18 GHz. To reduce errors, all values were obtained by averaging over the data measured from three different toroids of each sample.

2.5. Infrared emissivity measurement

Aluminum sheet, previously degreased in diluted NaOH at 50 °C and then chemically polished in diluted HNO_3, was used as the substrate for the coatings, and EPDM dissolved in dimethylbenzene as the adhesive. The prepared powder was used as the filling and its weight ratio was set as 30% in the coating. The coating thickness was controlled at about 35 μm by the wire-wound rod coater (Tianjin Jingke Material Testing Machine Factory, China). Infrared emissivity value at the wavelength of 8–14 μm was measured by using IR-2 Infrared Emissometer (Shanghai Institute of Technological Physics of the Chinese Academy of Sciences). All values were obtained by averaging over the data measured from ten different regions of each coating.

3. Results and discussion

3.1. Preparation of mesoporous C–TiO_2 nanocomposites

Small-angle XRD patterns of mesoporous C–TiO_2 nanocomposites with different calcined temperatures are shown in Fig. 1a. After the calcination under an inert atmosphere (N_2) at 350 °C for 5 h, the small-angle XRD pattern becomes poorly resolved, and a well-resolved diffraction peak is observed, suggesting that the typical ordered mesostructure is retained. Sample MC5T5-500 show patterns with an intense diffraction peak (100) and two

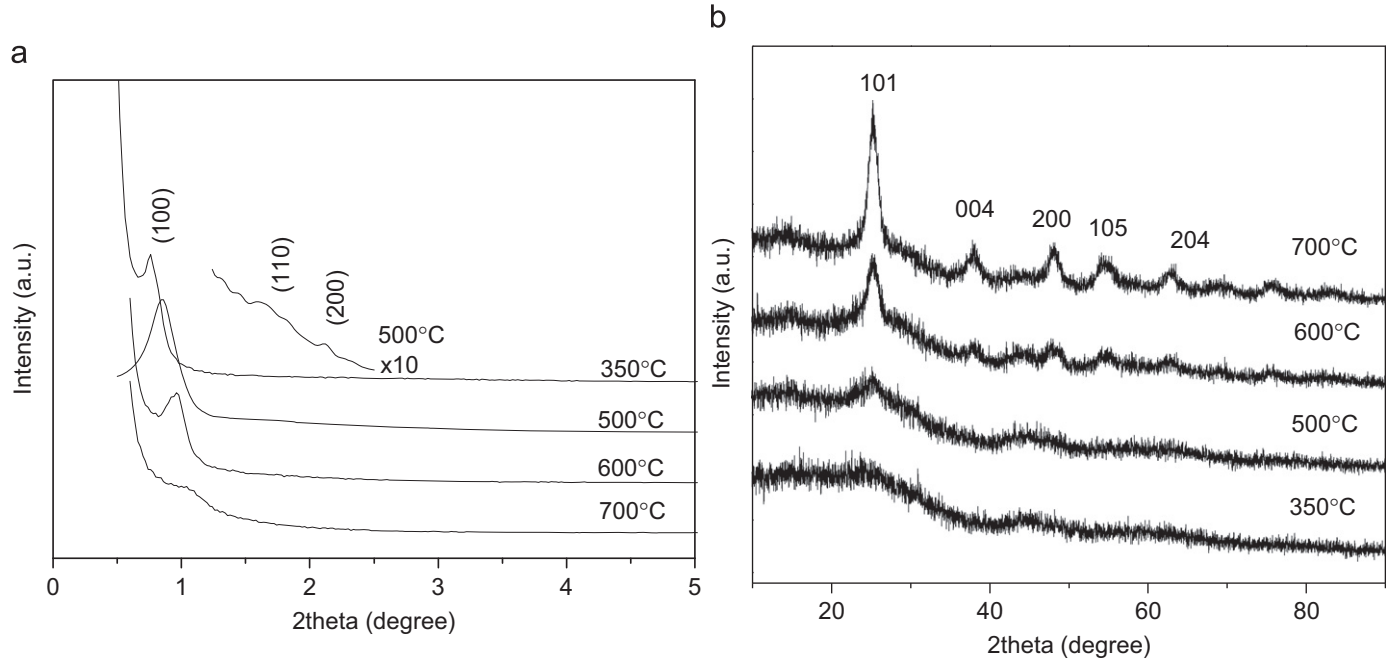

Fig. 1. (a) Small-angle XRD and (b) wide-angle XRD patterns of mesoporous C–TiO_2 nanocomposites MC5T5 calcined at 350, 500, 600 and 700 °C.

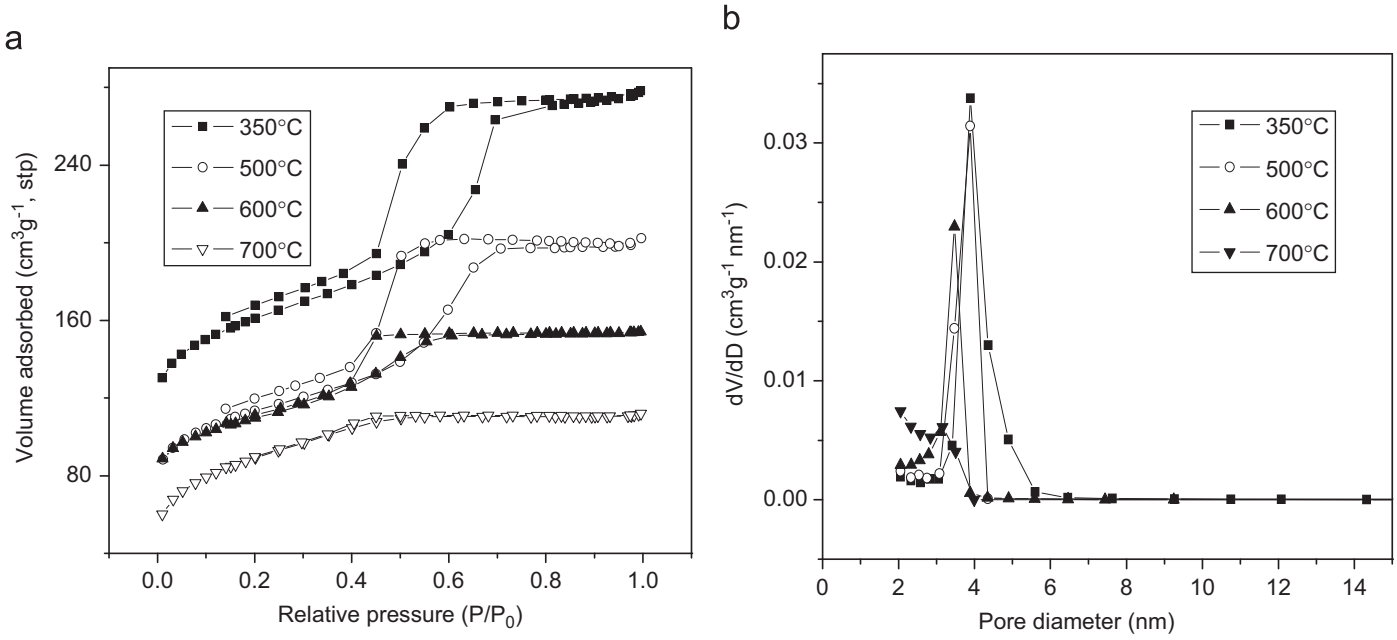

Fig. 2. N_2 adsorption–desorption isotherm (a) and pore size distribution (b) of mesoporous C–TiO_2 nanocomposites MC5T5 calcined at 350, 500, 600 and 700 °C in N_2. For clarity, the isotherms (a) for the MC5T5-350, MC5T5-500 and MC5T5-600 are offset vertically by 90, 40 and 40 $cm^3\ g^{-1}$, respectively.

weak peaks, (110) and (200), indicating an ordered 2D hexagonal mesoporous structure. The degradation of the mesostructure is related to the elimination of the copolymer template and the formation of nanocrystalline anatase in the frameworks during the thermal treatment process [38]. Furthermore, the 100 peak shifts toward higher angle. After the calcination temperature reaches 700 °C, the small-angle XRD pattern becomes more poorly resolved and the intensity of the X-ray diffraction peak greatly decreases, suggesting that the mesostructure regularity further degrades. The wide-angle XRD pattern of mesoporous nanocomposite heated at 350 °C reveals a low degree partial crystal and shows five broad diffraction peaks, indexed as 101, 004, 200, 105 and 204 reflections of anatase phase (Fig. 1b) after heated at 600 °C.

Fig. 2 shows N_2 sorption isotherms and pore size distributions of the C–TiO_2 nanocomposites calcined at different temperatures. The nanocomposites exhibit representative type IV isotherms with H_1 type hysteresis loops [1]. The mesoporous nanocomposite C–TiO_2-350 has a surface area of 253 $m^2\ g^{-1}$ and a pore volume of 0.28 $cm^3\ g^{-1}$. The other physicochemical properties of the mesoporous C–TiO_2 nanocomposites are shown in Table 1. A more detailed structural characterization is revealed by TEM images, as shown in Fig. 3. The calcined nanocomposite at 350 °C in N_2 shows large domains of highly ordered stripe-like and

hexagonally arranged images. These results indicate well-ordered hexagonal arrays of mesopores with 1-D channels [1]. After the nanocomposites are heated at 500 and 600 °C, the TEM images (Fig. 3c, d and e) also show well-defined hexagonal channels, suggesting that ordered mesostructures are retained, consistent with the results from the XRD patterns. After the nanocomposite is further heated at 700 °C, the mesostructure collapses partially.

We also attempt to prepare pure TiO_2 with ordered mesostructure by removing the carbon via the calcination in air. The mesoporous TiO_2 from mesoporous C–TiO_2-350 nanocomposite exhibits a pore size of 3.2 nm, a surface area of 205 $m^2\,g^{-1}$ and a pore volume of 0.17 $cm^3\,g^{-1}$. In the TEM image (Fig. 3g), we can see the partial ordered structure in the mesoporous TiO_2 material. After the carbon was burned off at 350 °C, XRD and nitrogen sorption techniques of the mesoporous TiO_2 material are in supplementary information (Figs. S1 and S2). It is worthy to note that mesoporous TiO_2 material shows an anatase phase without the carbon (Fig. S1). The mass percentages of C–H–O% and TiO_2% are 56% and 44%, respectively, in the ordered mesoporous C–TiO_2-350 nanocomposite, determined from TG result (Fig. S3).

The ratios of C/TiO_2 in the nanocomposites can be easily tuned by varying the mass ratios of resol to tetrabutyl titanate in triconstituent co-assembling process. N_2 adsorption/desorption isotherms of the nanocomposites with the different C/TiO_2 ratios are shown in Fig. 4a. All C–TiO_2 nanocomposites exhibit similar type IV curves with distinct capillary condensation steps, corresponding to a narrow

Table 1
Physicochemical properties of the mesoporous C–TiO_2 nanocomposites prepared from triconstituent co-assembly via EISA (evaporation-induced self-assembly) method, and of the corresponding mesoporous titania after the removal of carbon.

Sample	Pore size (nm)	Pore volume ($cm^3\,g^{-1}$)	BET area ($m^2\,g^{-1}$)	Mesopore area ($m^2\,g^{-1}$)
MC5T5-350	4.6	0.29	253	230
MC5T5-500	3.9	0.25	255	198
MC5T5-600	3.0	0.18	239	163
MC5T5-700	2.3	0.17	306	211
MC5T5-350-T	3.2	0.17	205	205
MC7T3-500	5.5	0.24	173	164
MC3T7-500	3.6	0.22	244	183

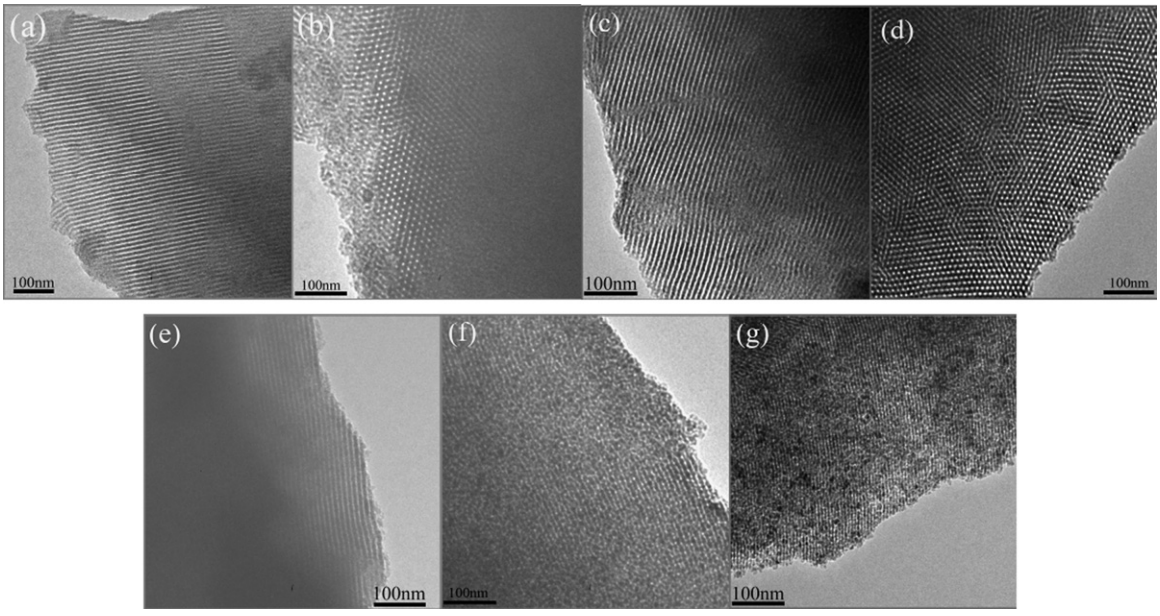

Fig. 3. TEM image of mesoporous C–TiO_2 nanocomposites calcined at 350 °C (a and b), 500 °C (c and d), 600 °C (e) and 700 °C (f) in N_2, mesoporous TiO_2 (g) calcined at 350 °C in air from C–TiO_2-350, viewed from the [110] (a, c, e, f and g) and [001] (b and d) directions.

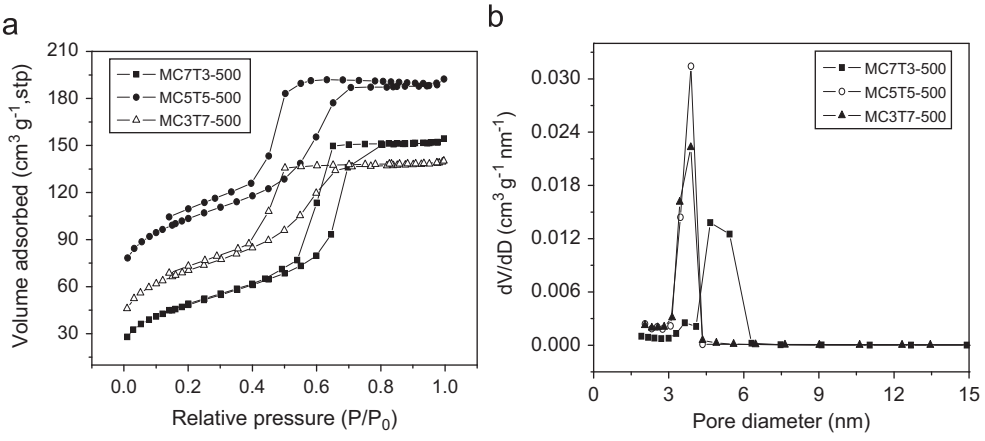

Fig. 4. N_2 adsorption/desorption isotherms (a) and the corresponding pore size distribution (B) for mesoporous C–TiO_2 nanocomposites with different TiO_2 content.

mesopore size distribution. TEM images (Fig. 5) further confirm that the nanocomposites with low TiO_2 content (30 and 50 wt%) have well-ordered mesostructures. In contrast, the mesostructure of the MC3T7 is partially destroyed as calcinated at 500 °C. It further provides evidence that the incorporation of carbon can effectively improve the thermal stability of mesoporous nanocomposites.

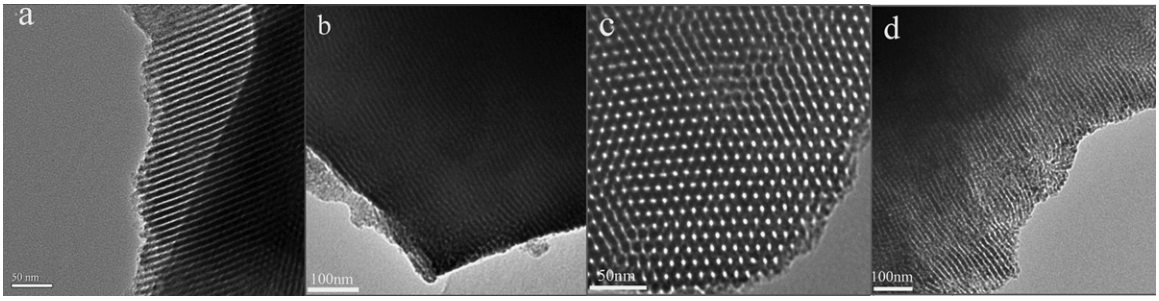

Fig. 5. TEM images of mesoporpus C–TiO_2 nanocomposites: (a) MC7T3-500; (b, c) MC5T5-500; (d) MC3T7-500.

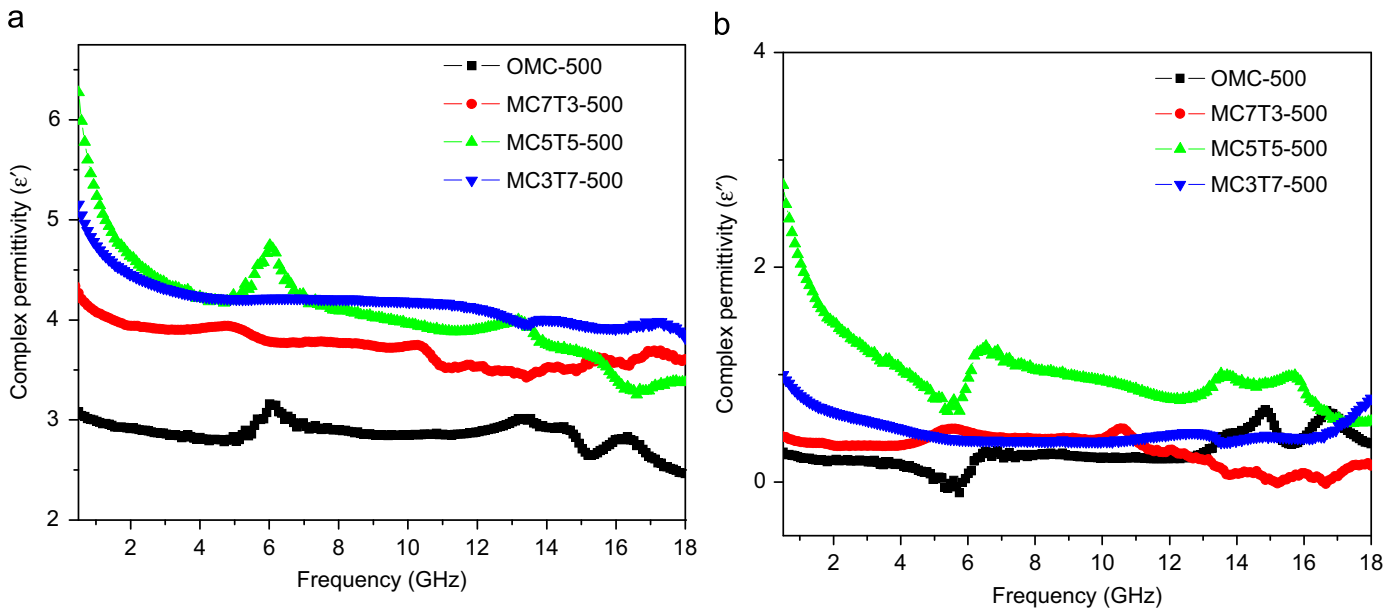

Fig. 6. Real (a) and imaginary (b) parts of the complex relative permittivity of the nanocomposites in the frequency range 0.5–18 GHz.

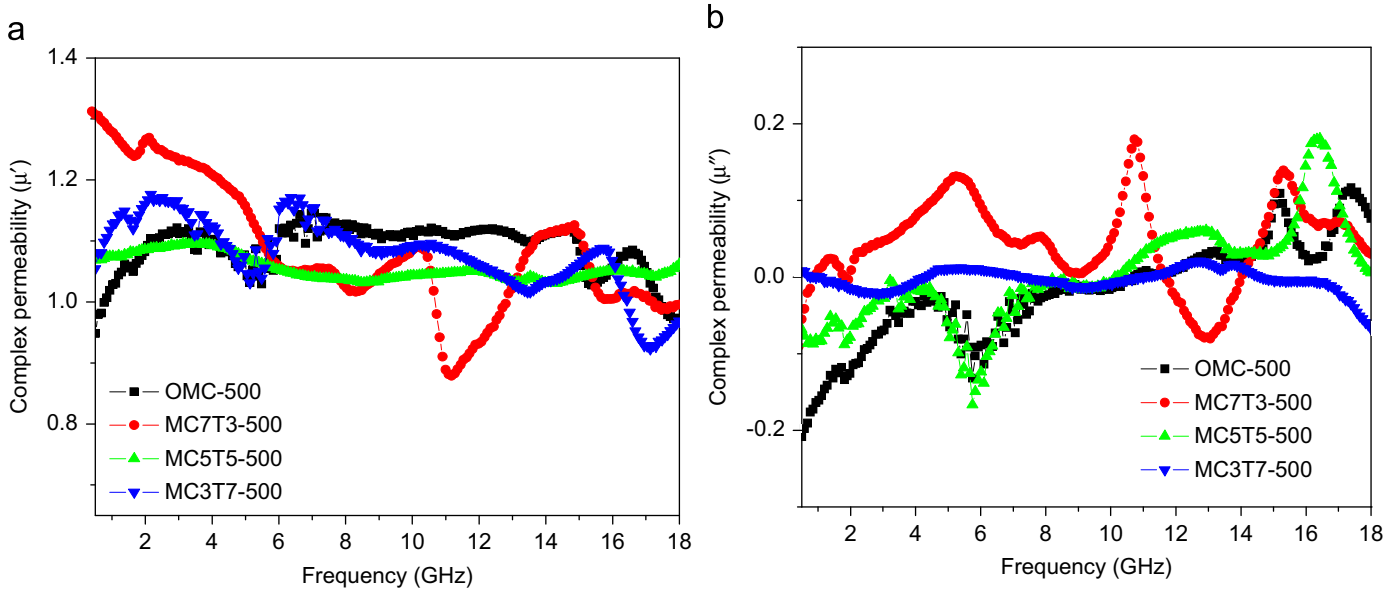

Fig. 7. Real (a) and imaginary (b) parts of the complex relative permeability of the nanocomposites in the frequency range 0.5–18 GHz.

3.2. Microwave adsorption properties

In order to investigate the intrinsic reasons for microwave absorption of the ordered mesoporous C–TiO_2 nanocomposites, we measured the complex permittivity and permeability of the epoxy resin/MCT-500 samples and the epoxy resin/OMC-500 with method of the coaxial line. Fig. 6a shows the real part (ε') and imaginary part (ε'') of complex permittivity of the epoxy resin/OMC-500 and resin/MCT-500 samples in the frequency range 0.5–18 GHz. The amount TiO_2 increases as the amount carbon decreases in the composites. Because the high dielectric constant of TiO_2 and the good thermal stability of polymer, the polymer-TiO_2 nanocomposites yield high dielectric constant [35]. It can be observed that the values of ε' and ε'' of the epoxy resin/OMC-500 sample are smaller than those of the epoxy resin/MCT-500 samples. Thereinto, the real permittivity of the epoxy resin/MC7T3-500 is smaller than that of the epoxy resin/MC5T5-500 and the epoxy resin/MC3T7-500. The real part values of relative dielectric permittivity for the epoxy resin/MCT-500 samples are comparatively smaller than those for the C-metal or C-oxides composites as reported in the literature [46–49]. The lower real part value of complex relative dielectric permittivity is a great advantage to strike a balance between permeability and permittivity, thus decreasing the reflection coefficient of the absorber compared with other metal magnetic materials for microwave absorbing application. The imaginary permittivity of the epoxy resin/OMC-500, the epoxy resin/MC3T7-500 and the epoxy resin/MC7T3-500 sample is below 1, which indicates very poor dielectric loss. Fig. 7a and b depict the variation of the real part (μ') and imaginary part (μ'') with frequency in the 0.5–18 GHz. The real permeability of the epoxy resin/OMC-500 and all the epoxy resin/MCA-700, is around 1.1 and nearly independent of frequency, whereas the μ'' values give peaks in the range 14–18 GHz except the epoxy resin/MC3T7-500. From the results of measurements for relative permittivity and permeability, it can be expected that the ordered mesoporous C–TiO_2 nanocomposites give good microwave absorption properties at high frequency range.

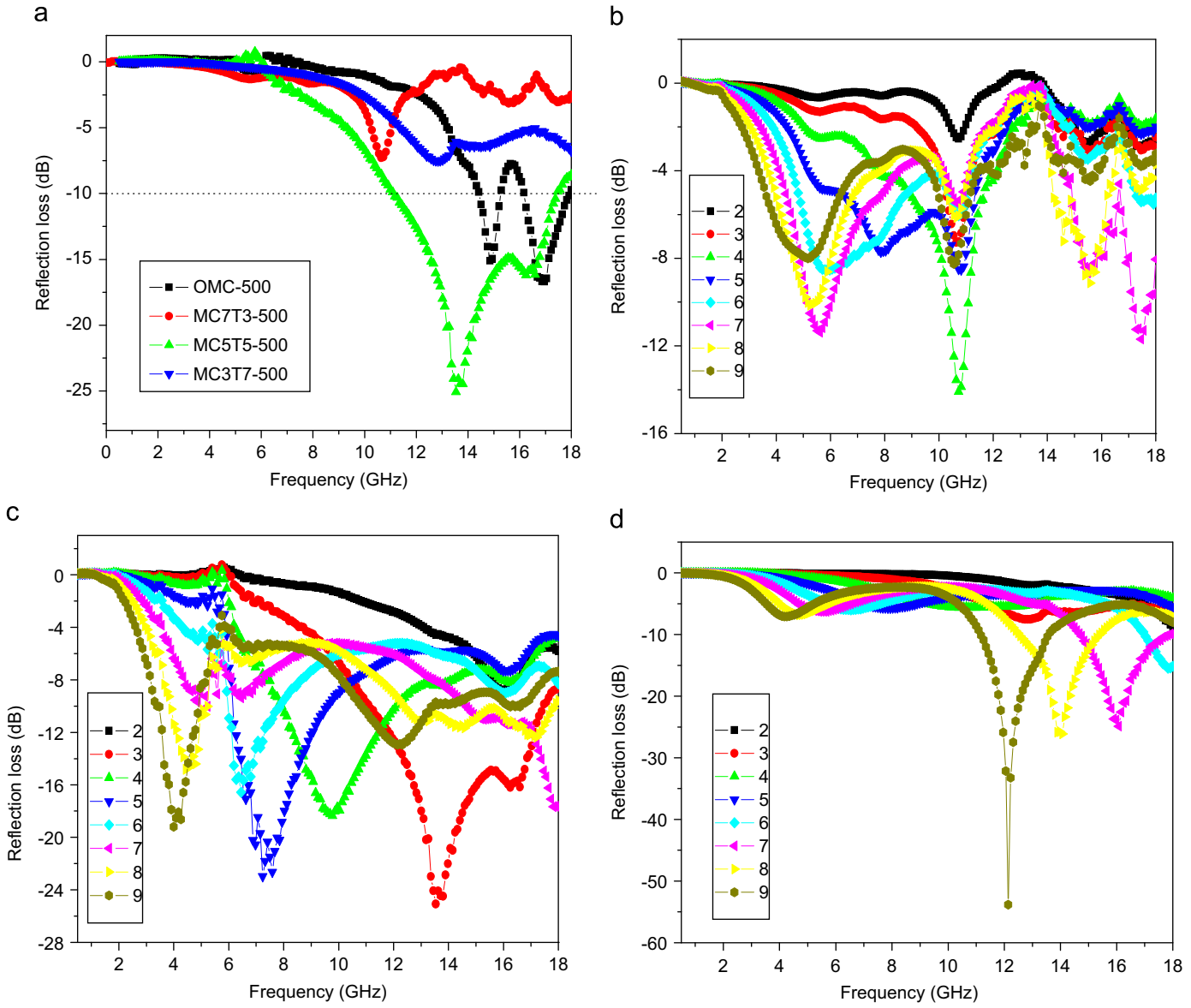

Fig. 8. (a) Reflection loss for the nanocomposites and OMC-500, with a sample thickness of 3 mm in the frequency range 0.5–18 GHz. Reflection loss for the MC7T3 (b), MC5T5 (c) and MC3T7 (d) with different thickness (2, 3, 4, 5, 6, 7, 8 and 9 mm) in the frequency range 0.5–18 GHz. In measurement, 40 wt% sample and 60 wt% epoxy resin were used.

The reflection loss (*RL*) of microwave was calculated from the relative permeability and permittivity at the given frequency and absorber thickness using the following equations [50,51]:

$$RL = 20\log|(Z_{in}-Z_0)+(Z_{in}+Z_0)| \quad (1)$$

$$Z_0 = \sqrt{\frac{\mu_0}{\varepsilon_0}} \quad (2)$$

$$Z_{in} = Z_0\sqrt{\frac{\mu_r}{\varepsilon_r}}\tanh\left[j\frac{2\pi fd}{c}\sqrt{\mu_r\varepsilon_r}\right] \quad (3)$$

where μ_0 and ε_0 are the complex relative permeability and permittivity of free space, Z_0 is the impedance of free space, Z_{in} is the input impedance of absorber, μ_r and ε_r are the complex relative magnetic permeability and dielectric permittivity of the composite medium, respectively, f is the frequency of the microwave, d is the thickness of an absorber and c is the velocity of microwave.

Fig. 8a shows the reflection loss of the epoxy resin/OMC-500 and epoxy resin/MCT-500 samples with a thickness of 3.0 mm in 0.5–18 GHz. The maximum *RL* value for the epoxy resin/OMC-500 is measured to be −16.8 dB at 16.9 GHz. The epoxy resin/MCT-500 samples exhibit wide frequency absorption characteristics. The relative absorption peaks are about −7.4, −25.4 and −7.9 dB and the bandwidths lower than −10 dB are 0, 6.6 and 0 GHz for the samples with increasing TiO_2 contents, respectively, as the layer thickness is 3 mm. The poor microwave absorption property displayed by the epoxy resin/MC3T7-500 and the epoxy resin/MC7T3-500 may be due to the poor dielectric content and lower mesoporous aera (164 and 183 $m^2\,g^{-1}$). The incident microwaves are confined within the porous structure of absorbers and multiple reflections induce the energy dissipation occurring in many different sites [48,52,53]. The calculated results with different thicknesses of the absorbers are shown in Fig. 8(b, c, d), which indicate that the epoxy resin/MC5T5-500 with the larger dielectric content shows interesting microwave absorption property compared with those of lower dielectric constants (TiO_2: 30% and 70%). Obviously, when the thicknesses of the epoxy resin/MCT-500 samples increase, the absorption peaks become sharper and shift to lower frequency. Increasing the epoxy resin/MC3T7-500 thickness to 7 mm another strong absorption peak appears. The matching thickness of the epoxy resin/MC7T3-500, the epoxy resin/MC5T5-500 and the epoxy resin/MC3T7-500 are thus 4, 3 and 9 mm, respectively. The μ'' of the mesoporous C–TiO_2 nanocomposites and OMC-500 are almost zero. So the microwave absorptions of the mesoporous nanocomposites and OMC-500 are resulted mainly from dielectric loss rather than magnetic loss. In general, the excellent microwave absorptions are strongly dependent on the efficient complementarities between the relative permittivity and permeability. Only magnetic loss or dielectric loss leads to weak electromagnetic attenuation [35]. Hence, we can see that reflection loss exceeding −10 dB can be obtained for all frequencies within the 3.3–18 GHz range by choosing an appropriate layer thickness between 2 and 9 mm and a seemly TiO_2 content.

The mechanism of microwave absorption, effect of structural anisotropy on absorption is discussed as follows. The hexagonally ordered mesopores in the nanocomposites are robust and interconnected, and incident microwaves could take place energy dissipation many times, in the form of reflection and scattering confined within the nanostructure [44,45,47,52]. In such ordered materials, the microwave absorption properties are expected to be anisotropic in nature. It is reasonable to say that the ordered mesoporous framework endows the resonance loss. Therefore, ordered mesoporous C–TiO_2 nanocomposites exhibit excellent electromagnetic properties, which are attributed to the electromagnetic match in microstructure and the strong natural resonance. MC5T5-500 has best ordered mesoporous structure with the bigger pore volume and BET aera than those of MC3T7-500 and MC7T3-500 (Table 1), which indicates that MC5T5-500 has a better orientation and a bigger absorption intensity (Fig. 8a).

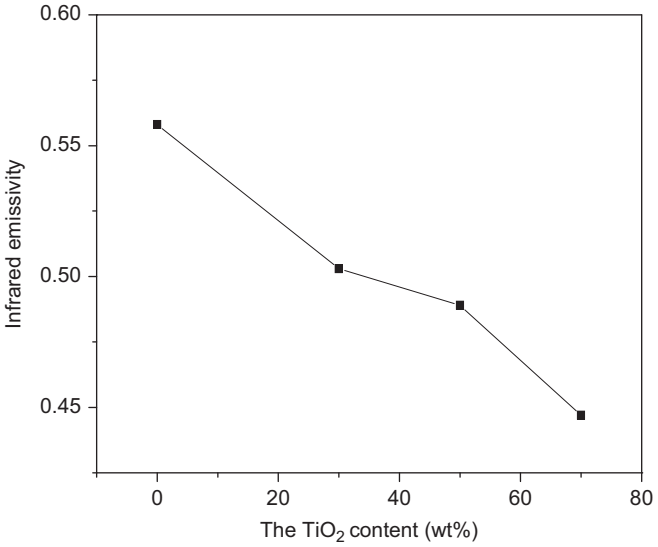

Fig. 9. The average infrared emissivity at 8–14 μm of the coatings (OMC-500, MC7T3-500, MC5T5-500 and MC7T3-500) with a thickness of 34 μm using EPDM as an adhesive.

3.3. Infrared emissivity

Fig. 9 indicates the infrared emissivity curves of the nanocomposites with different TiO_2 contents. The results show that the input of the TiO_2 made the infrared emissivity of the nanocomposite fall sharply and the infrared emissivity reach the lowest value of 0.447 when the TiO_2 content was 70 wt%. We can interpret the results of experiments as follows. According to Kirchhoff's law, the sum of the emissivity and reflectivity is 1 for the opacity materials. The reflectivity of TiO_2 is higher than carbon, which means TiO_2 has lower emissivity. Besides, surface effect and microdimension effect of the mesoporous material also lead to the decrease of infrared emissivity. So the TiO_2 can adjust the infrared emissivity of nanocomposite. However, too many TiO_2 constituents reduce the microwave absorption characteristics. Consequently, based on the above discussion, the optimal content of TiO_2 should be kept at 50 wt% in the nanocomposite for excellent microwave absorbing properties and low infrared emissivities.

4. Conclusions

In summary, we demonstrate a facile synthesis of ordered mesoporous C–TiO_2 nanocomposites with crystalline framework through a simple sol–gel process and evaporation-induced triconstituent co-assembly effect. By regulating the ratios of C/TiO_2, one can control the reflection loss and infrared emissivity of the nanocomposites. The relative absorption peaks are about −7.4, −25.4 and −7.9 dB and the bandwidths lower than −10 dB are 0, 6.6 and 0 GHz for the MC7T3-500, MC5T5-500 and MC3T7-500, respectively, as the layer thickness is 3 mm. Microwave absorbing properties can be modulated simply by controlling the thickness of the samples for the required frequency bands. The ordered C–TiO_2 nanocomposite obtained at 500 °C with a pore of

3.9 nm, pore volume of 0.25 $cm^3 g^{-1}$, and surface area of 255 $m^2 g^{-1}$ displays a good microwave absorbing ability, especially in the high-frequency range and also has a low infrared emissivity of 0.489. The material can be considered as a good lightweight candidate for microwave absorption and infrared camouflage, simultaneously.

Acknowledgments

The project was supported by the National Natural Science Foundation of China (50871053) and the Aeronautical Science Foundation of China (2007ZF52061).

Appendix A. Supplementary information

Supplementary data associated with this article can be found in the online version at doi:10.1016/j.jssc.2010.09.028.

References

[1] C.T. Kresge, M.E. Leonowicz, W.J. Roth, J.C. Vartuli, J.S. Beck, Nature 359 (1992) 710.
[2] J.S. Beck, J.C. Vartuli, W.J. Roth, M.E. Leonowicz, C.T. Kresge, K.D. Schmitt, C.T.-W. Chu, D.H. Olson, E.W. Sheppard, S.B. McCullen, J.B. Higgins, J.L. Schlenker, J. Am. Chem. Soc. 114 (1992) 10834.
[3] J.H. Zhou, J.P. He, Y.J. Ji, W.J. Dang, X.Lei. Liu, G.W. Zhao, C.X. Zhang, J.S. Zhao, Q.B. Fu, H.P. Hu, Electrochim. Acta 52 (2007) 4691.
[4] A. Taguchi, F. Schuth, Micropor. Mesopor. Mater. 77 (2005) 1.
[5] S.M. Zhu, H.S. Zhou, T. Miyoshi, M. Hibino, I. Honma, M. Ichihara, Adv. Mater. 16 (2004) 2012.
[6] M. Okumura, S. Tsubota, M. Iwamoto, M. Haruta, Chem. Lett. 4 (1998) 315.
[7] C.H. Huang, D. Gu, D.Y. Zhao, R.A. Doong, Chem. Mater. 22 (2010) 1760.
[8] Z.X. Wu, Y.X. Yang, D. Gu, Q. Li, D. Feng, Z.X. Chen, B. Tu, P.A. Webley, D.Y. Zhao, Small 5 (2009) 2738.
[9] R.L. Liu, Y.F. Shi, Y. Wan, Y. Meng, F.Q. Zhang, D. Gu, Z.X. Chen, B. Tu, D.Y. Zhao, J. Am. Chem. Soc. 128 (2006) 11652.
[10] R.L. Liu, Y.J. Ren, Y.F. Shi, F. Zhang, L.J. Zhang, B. Tu, D.Y. Zhao, Chem. Mater. 20 (2007) 1140.
[11] X.F. Qian, Y. Wan, Y.L. Wen, N.G. Jia, H.X. Li, D.Y. Zhao, J. Colloid Interface Sci. 328 (2008) 367.
[12] T. Wang, J.P. He, C.X. Zhang, J.H. Zhou, Y.X. Guo, Chen, X.Z.Y. Di, D. Sun, D.J. Wang, Acta Phys.-Chim. Sin 24 (2008) 2314.
[13] J.H. Zhou, J.P. He, T. Wang, D. Sun, G.W. Zhao, X. Chen, D.J. Wang, Z.Y. Di, J. Mater. Chem. 18 (2008) 5776.
[14] S. Geetha, K.K.S. Kumar, D.C. Trivedi, Compos. Sci. Technol. 65 (2005) 973.
[15] D.S. Li, T. Horikawa, J.R. Liu, M. Itoh, K. Machida, J. Alloys Compd. 408 (2006) 1429.
[16] S. Motojimaa, S. Hoshiya, Y. Hishikawab, Carbon 41 (2003) 2653.
[17] J. Ma, J.F. Diehl, E.J. Johnson, K.R. Martin, N.M. Miskovsky, C.T. Smith, G.J. Weisel, B.L. Weiss, D.T. Zimmerman, J. Appl. Phys. 101 (2007) 074906.
[18] P. Xu, X.J. Han, C. Wang, D.H. Zhou, Z.S. Lv, A.H. Wen, X.H. Wang, B. Zhang, J. Phys. Chem. B 112 (2008) 10443.
[19] S.M. Abbas, A.K. Dixit, R. Chatterjee, T.C. Goel, J. Magn. Magn. Mater. 309 (2007) 20.
[20] G. Xie, Z. Wang, Z. Cui, Y. Shi, Carbon 43 (2005) 3181.
[21] J. Chen, Y.G. Wang, Z.Q. Li, C. Wang, J.F. Li, Y.J. Gu, J. Phys.: Conf. Ser. 152 (2009) 012041.
[22] Y.L. Yang, M.C. Gupta, Nano Lett. 5 (2005) 2131.
[23] H.M. Kim, K. Kim, C.Y. Lee, J. Joo, S.J. Cho, H.S. Yoon, D.A. Pejakovic, J.W. Yoo, A.J. Epstein, Appl. Phys. Lett. 84 (2004) 589.
[24] R.C. Che, L.M. Peng, X.F. Duan, Q. Chen, X.L. Liang, Adv. Mater. 16 (2004) 401.
[25] J. Deng, X. Ding, W. Zhang, Y. Peng, J. Wang, X. Long, P. Li, A.S.C. Chan, Polymer 43 (2002) 2179.
[26] G.Q. Wang, X.D. Chen, Y.P. Duan, S.H. Liu, J. Alloys Compd. 454 (2008) 340.
[27] J.R. Liu, M. Itoh, T. Horikawa, K. Machida, S. Sugimoto, T. Maeda, J. Appl. Phys. 98 (2005) 054305.
[28] Y. Xie, X. Zhao, Y. Li, Q. Zhao, X. Zhou, Q. Yuan, J. Solid State Chem. 181 (2008) 1936.
[29] R. Kun, S. Tarjan, A. Oszko, T. Seemann, V. Zollmer, M. Busse, I. Dekany, J. Solid State Chem. 182 (2009) 3076.
[30] S.K. Das, M.K. Bhunia, A. Bhaumik, J. Solid State Chem. 183 (2010) 1326.
[31] D.L. Li, H.S. Zhou, I. Honma, Nat. Mater. 3 (2004) 65.
[32] X. Chen, S.S. Mao, Chem. Rev. 107 (2007) 2891.
[33] H.S. Zhou, D.L. Li, M. Hibino, I. Honma, Angew. Chem. Int. Ed. 44 (2005) 797.
[34] J. Lee, M.C. Orilall, S.C. Warren, M. Kamperman, F.J. Disalvo, U. Wiesner, Nat. Mater. 7 (2008) 222.
[35] A. Dey, S. De, A. De, S.K. De, Nanotechnology 15 (2004) 1277.
[36] S.W. Phang, M. Tadokoro, J. Watanabe, N. Kuramoto, Polym. Adv. Technol. 6 (2009) 550.
[37] F. Pichot, J.R. Pitts, B.A. Gregg, Langmuir 16 (2000) 5626.
[38] Y. Meng, D. Gu, F.Q. Zhang, Y.F. Shi, H.F. Yang, Z. Li, C.Z. Yu, B. Tu, D.Y. Zhao, Angew. Chem. Int. Ed. 44 (2005) 7053.
[39] Y. Meng, D. Gu, F.Q. Zhang, Y.F. Shi, L. Cheng, D. Feng, Z.X. Wu, Z.X. Chen, Y. Wan, S. Andreas, D.Y. Zhao, Chem. Mater. 18 (2006) 4447.
[40] J.H. Wu, L.B. Kong, Appl. Phys. Lett. 84 (2004) 4956.
[41] Y. Shen, Y.H. Lin, M. Li, C.W. Nan, Adv. Mater. 19 (2007) 1418.
[42] X. Qi, Y. Yang, W. Zhong, Y. Deng, C. Au, Y. Du, J. Solid State Chem. 182 (2009) 2691.
[43] Z. Jia, Y. Duan, S. Li, X. Li, S. Liu, J. Solid State Chem. 183 (2010) 1490.
[44] T. Wang, J. He, J. Zhou, X. Di, J. Zhao, S. Wu, Y. Guo, Micropor. Mesopor. Mater. 134 (2010) 58.
[45] J. Zhou, J. He, G. Li, T. Wang, D. Sun, X. Ding, J. Zhao, S. Wu, J. Phys. Chem. C 114 (2010) 7611.
[46] T.N. Narayanan, V. Sunny, M.M. Shaijumon, P.M. Ajayan, M.R. Anantharaman, Electrochem. Solid-State Lett. 12 (2009) 21.
[47] X. Tang, Q. Tian, B. Zhao, K. Hu, Mater. Sci. Eng. A 445 (2007) 135.
[48] Q. Liu, D. Zhang, T. Fan, Appl. Phys. Lett. 93 (2008) 013110.
[49] D. Zhao, X. Li, Z.M. Shen, J. Alloys Compd. 471 (2009) 457.
[50] T. Maeda, S. Sugimoto, T. Kagotani, N. Tezuka, K. Inomata, J. Magn. Magn. Mater. 281 (2004) 195.
[51] E. Michielssen, J. Sajer, S. Ranjithan, R. Mittra, IEEE Trans. Electromagn. Wave Theory Tech. 41 (1993) 1024.
[52] J.C. Wang, C.S. Xiang, Q. Liu, Y.B. Pan, J.K. Guo, Adv. Funct. Mater. 18 (2008) 2995.
[53] X.H. Guo, Y.H. Deng, D. Gu, R.C. Che, D.Y. Zhao, J. *Mater. Chem.* 19 (2009) 6706.